Electromechanical Modulations in Transition Metal Dichalcogenide Nanosheets: Implications for Environmental Sensors

V. Bessa, Mauricio; D. Freitas, Wellington ; Paz Neme, Natália; G. P. Martins, Luiz; P. M. Barboza, Ana; J. S. Matos, Matheus ; S. C. Mazzoni, Mario; R. A. Neves, Bernardo

Published in:
ACS Applied Nano Materials

DOI:
10.1021/acsanm.1c03002

Publication date:
2021

ACS APPLIED NANO MATERIALS

www.acsanm.org Article

Electromechanical Modulations in Transition Metal Dichalcogenide Nanosheets: Implications for Environmental Sensors

Mauricio V. Bessa, Wellington D. Freitas, Natália P. Neme, Luiz G. P. Martins, Ana P. M. Barboza, Matheus J. S. Matos, Mario S. C. Mazzoni, and Bernardo R. A. Neves*

Cite This: *ACS Appl. Nano Mater.* 2021, 4, 11305–11311 Read Online

ACCESS | Metrics & More | Article Recommendations | Supporting Information

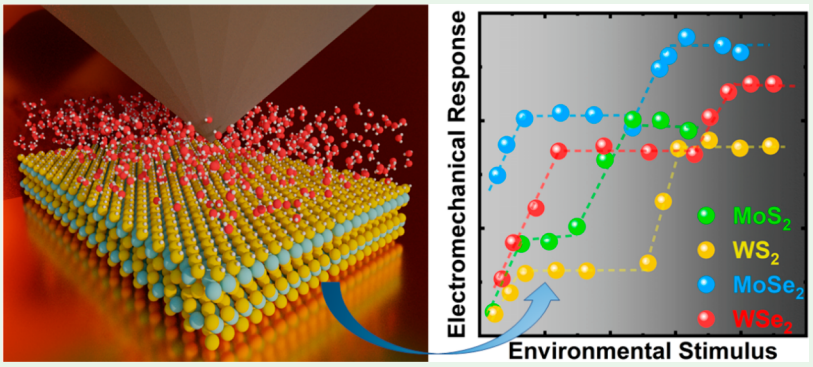

ABSTRACT: Transition metal dichalcogenides (TMDs) are key players in the two-dimensional materials nanoarena due to their exquisite optoelectronic properties under a standard environment (room temperature and atmospheric pressure). Nevertheless, as reported in the literature, they may also portray interesting physical properties under different environments. Here, we show two distinct and significant electromechanical modulations in TMD nanosheets which are tuned by the environmental conditions (applied pressure and adsorbents). Using scanning probe microscopy techniques, we modify the environmental conditions and observe steplike rises in the electrical response of all studied TMDs (MoS_2, WS_2, $MoSe_2$, and WSe_2—monolayers and few layers). *Ab initio* calculations enable full understanding of specific mechanisms behind these electromechanical modulations, which may find important applications in the design of TMD-based environmental sensors.

KEYWORDS: *transition metal dichalcogenides, scanning probe microscopy, DFT calculations, environment, pressure, MoS_2, WS_2, $MoSe_2$*

Transition metal dichalcogenides (TMDs) offer a plethora of possible applications due to their different composition-specific properties, constituting one of the most versatile classes of two-dimensional (2D) materials.[1−3] But rather than their specificities, it is their general common properties that make TMDs important commodities for the ongoing 2D revolution.[1−3] One example is their interesting electromechanical behavior, where pressure-induced gap closure was initially predicted[4−8] and recently observed[9−12] for several TMDs. In these previous works, the pressure effect was associated with a compression of the TMD layer (altering the metal−chalcogen bond angle) in combination with a layer−layer approximation (for the case of multilayered TMDs).[4−12] In another set of environment-related studies, it was initially theoretically proposed[13−15] and later observed experimentally[16−18] that surface modification with hydrogen may induce different magnetic and electric responses of the functionalized TMDs, suggesting the emergence of ferromagnetic and/or conducting states.[13−18] Here, using scanning probe microscopy (SPM) techniques and *ab initio* calculations, we identify two distinct environment-controlled electromechanical modulations that occur unconnectedly in monolayer (ML) and few-layer (FL) nanosheets of four different TMDs: MoS_2, WS_2, $MoSe_2$, and WSe_2. In a pressure-dependent experiment, we observe an initial electrical response modification at low pressure values (which requires previous exposure to an ambient atmosphere) that is followed by a second modification at higher pressure values (which occurs even without previous exposure to an ambient atmosphere). Experimentally, such electromechanical modulations are characterized by increasing plateaus in the charge injection efficiency, which normally are a signature for gap closure and/or conducting states availability.[19−22] Even though some previous studies have reported on a single environment-related modification of TMDs (either

Received: September 17, 2021
Accepted: September 23, 2021
Published: October 6, 2021

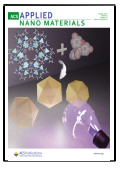

https://doi.org/10.1021/acsanm.1c03002
ACS Appl. Nano Mater. 2021, 4, 11305−11311

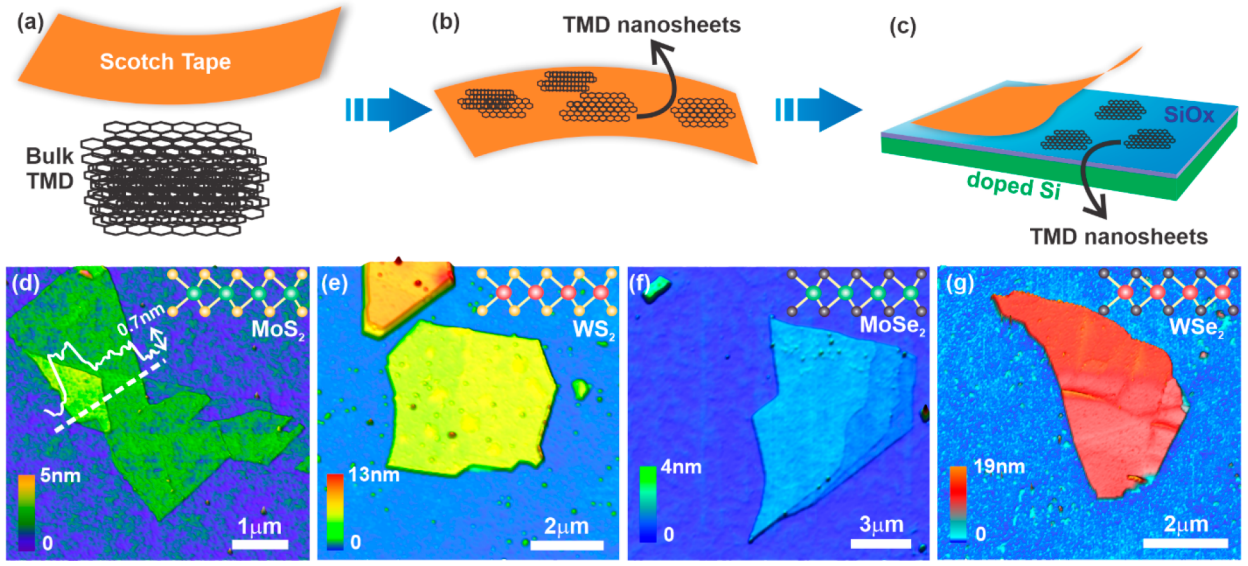

Figure 1. Exfoliation process of TMD nanosheets and their atomic force microscopy images: (a) Schematic drawing of the mechanical exfoliation process, where adhesive tape is used to mechanically peel TMD nanosheets from a bulk precursor, as shown in (b). (c) TMD nanosheets are transferred onto a doped Si substrate (in green shades) covered by a thin (300 nm) layer of Si oxide (in blue shades). AFM images of some TMD nanosheets: (d) MoS_2 (green shades), (e) WS_2 (yellow shades), (f) $MoSe_2$ (blue shades), and (g) WSe_2 (red shades). The schematics at the top right figures (d–g) illustrate the chemical structure of each compound (Mo atoms: green; W atoms: red; S atoms: yellow; Se atoms: gray). Scale bars indicate lateral and vertical dimensions.

pressure-related[4−12] or adsorbent-related[13−18]), to our knowledge, the concomitant observation of two distinct environment-related modifications has never been reported. Therefore, the origins of each modification must be identified and any eventual interplay between them investigated. Our *ab initio* calculations indicate that the first transition is associated with pressure-induced hydrogenation of the chalcogen atom, which results in available conducting states.[13−18] In the environment of our experiment, water, from the ubiquitous contamination layer atop the samples originated from any previous exposure to ambient atmosphere, is believed to be the current H source.[19−22] The second modification, observed at high pressures, is associated with both layer−layer approximation (for FL flakes) and bond-angle modification (for both ML and FL flakes).[4−12] These distinct processes, which are now concomitantly observed in a single experiment, evidence the unique environment-related electromechanical behavior of TMD nanosheets.

Figure 1 illustrates the mechanical exfoliation process used to produce the TMD nanosheets investigated in this work and also shows atomic force microscopy (AFM) images of some of them. They were prepared by conventional mechanical exfoliation using adhesive tape (Figure 1a) to peel nanosheets from a bulk TMD mineral precursor. These nanosheets attached to the tape (Figure 1b) are transferred onto a 300 nm thick Si oxide layer covering the p-doped Si substrate (Figure 1c).[1−3] Monolayer, bilayer, and few-layer flakes were initially identified by using optical microscopy and, then, imaged via AFM. Figures 1d, 1e, 1f, and 1g show MoS_2, WS_2, $MoSe_2$, and WSe_2 micrometer-scale flakes atop the Si oxide substrate, respectively. In Figures 1d–g, the insets at their top right indicate schematic chemical structures of the investigated TMDs. Figure 1d also shows a line profile indicating that a large fraction of this MoS_2 flake is a monolayer. On the other hand, the $MoSe_2$ flake in Figure 1f is comprised by monolayer, bilayer, and trilayer regions (from the rightmost to the center of the image). Both WS_2 and WSe_2 flakes, in Figures 1e and 1g, are few-layered (FL) nanosheets.

Recently, we have applied a SPM-based electromechanical characterization protocol to investigate interesting processes such as the semiconductor−metal transition in carbon nanotubes,[19] a diamondization mechanism in graphene,[20] and even the formation of a h-BN-based conducting material.[21] Thus, motivated by these previous achievements and the reported pressure-induced gap closure in TMDs,[4−12] we decided to apply such SPM protocol to further investigate these materials. Within this methodology, eventual electromechanical effects are investigated via a biased electrostatic force microscopy (EFM) tip that is used to simultaneously apply forces and inject charges on all TMD flakes.[19−21] Subsequent EFM imaging monitors transferred charges, evidencing any pressure-induced effects on the electrical properties of the material under investigation. Additionally, the sample atmosphere and temperature can be controlled via a homemade environmental chamber and an *in situ* heater, enabling the investigation of additional environment-related parameters.[19−22]

Figure 2 summarizes the environment-dependent SPM electromechanical results. As described above, the initial experiment in Figure 2a monitors the tip−sample charge transfer efficiency as a function of the applied tip−sample force for FL flakes of all TMDs (a graphene monolayer, MLG, was also investigated as a reference[20]) at dry atmosphere and room temperature. All samples were initially submitted to ambient humidity (~50% relative humidity, RH), which is enough to create an omnipresent water contamination layer fully covering the sample surface at room temperature[19−21] (see the Supporting Information). In the experiment itself, a biased tip applies a desired force onto the investigated flake and, at the same time, inject charges into it. The extent of transferred charges is subsequently determined via a conventional EFM imaging procedure[19−22] (see the Supporting Information).

https://doi.org/10.1021/acsanm.1c03002
ACS Appl. Nano Mater. 2021, 4, 11305−11311

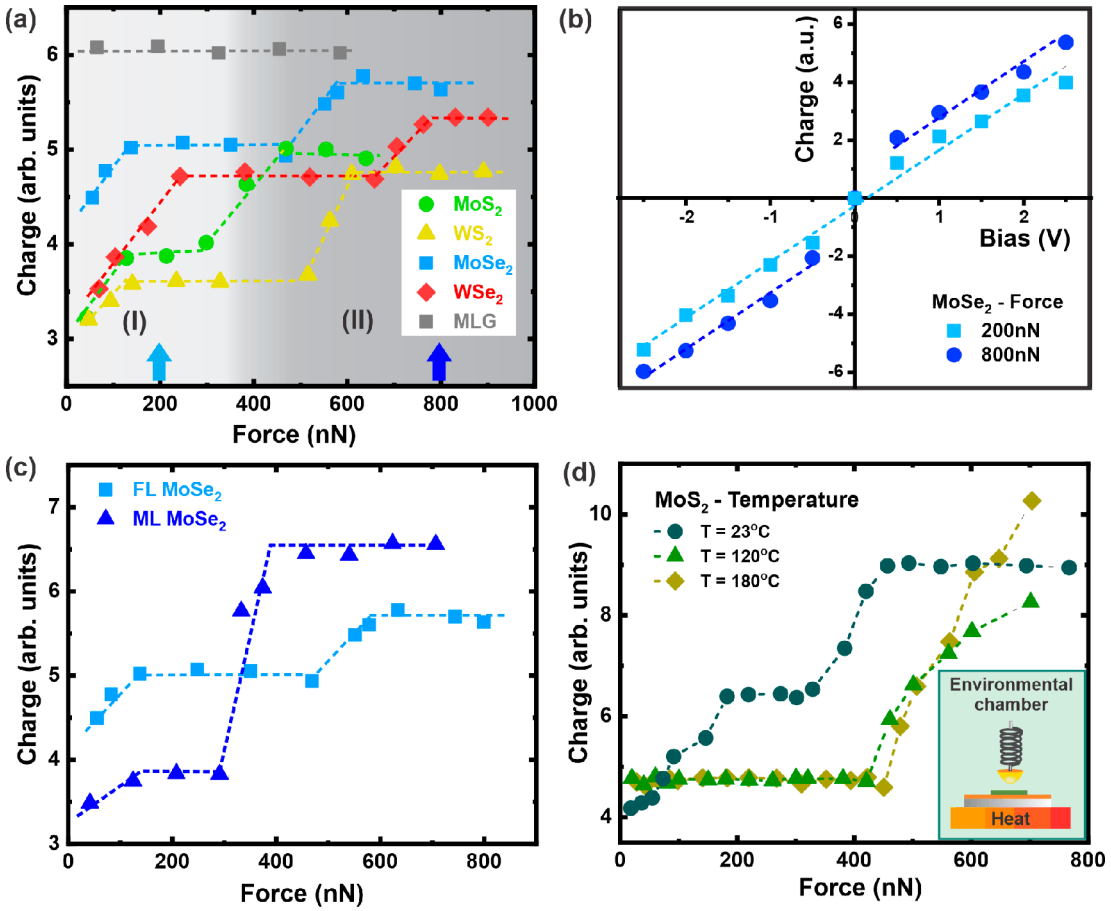

Figure 2. Environment-dependent charge injection experiments on TMDs. (a) Injected charge as a function of applied force at fixed tip bias (V = −4 V) for different few-layered TMDs and monolayer graphene at dry atmosphere and room temperature (after sample exposure to ambient atmosphere). (b) Injected charge as a function of applied tip bias V at fixed forces (200 nN: light blue squares; 800 nN: dark blue circles) for a FL $MoSe_2$ flake at the same environmental conditions of (a). (c) Injected charge as a function of applied force for ML and FL $MoSe_2$ flakes at the same environmental conditions of (a). (d) Injected charge as a function of applied force for a FL MoS_2 flake at different temperatures in a dry atmosphere: green circles, 23 °C; green triangles, 120 °C; green diamonds, 180 °C. Inset: scheme of the environment control setup. All dashed lines in all graphs are guides for the eye only.

Therefore, the result of this experiment is a plot of injected charges as a function of applied force for all TMDs investigated in this work and the reference MLG flake. As shown in Figure 2a, all TMD FL flakes present a similar behavior: injected charges quantity initially increases with the applied force (pressure) until it stabilizes in a first plateau. This first plateau is achieved at applied forces around the 200−300 nN range for all four TMDs (region I in Figure 2a, light gray shade). Increasing the applied force beyond these values gives rise to a second increase in charge transfer efficiency followed by a second plateau. Again, despite differences on individual force onset values, this second rise and plateau is common to all FL TMDs (region II in Figure 2a, gray shade). In contrast, the charge transfer efficiency in the graphene monolayer does not have any dependence with the applied force (gray squares).

In other words, as expected, the electronic properties of MLG are not altered by the tip−sample pressure within the range shown in Figure 2a.[20] The results in Figure 2a were obtained by using a fixed tip bias V = −4 V during charge injection (see the Supporting Information for further details). To investigate the influence of tip bias (or electric field) on the processes observed in Figure 2a, an additional experiment was performed to monitor the charge transfer as a function of tip bias while keeping the applied force (pressure) constant and at the same environmental conditions of Figure 2a.

Figure 2b shows the results for the $MoSe_2$ FL flake under two distinct applied force conditions: 200 and 800 nN; see blue arrows in Figure 2a (similar results were obtained for other TMDs; data not shown). For the low-force regime (light blue squares in Figure 2b), there is an evident linear dependence of the charge q with bias V, which is a signature of a capacitive charging behavior $q = CV$, where C is the system capacitance.[19] The data for high applied force (dark blue circles) also show an approximate linear behavior (apart from small biases) with a similar slope to the low-force case (similar differential capacitance). There is also a small deviation from linearity at large positive tip biases, which is simply associated with a limitation of the experimental setup.[19−21] To avoid it, in all experiments (Figure 2 and Figures S1−S6), a negative tip bias was used. Nevertheless, the important feature of Figure 2b is that the charging efficiency is larger for larger applied forces, regardless tip bias (electric field intensity and direction). In other words, the results shown in Figure 2a are robust against electric field intensity and direction.

Another interesting question is whether the processes observed for few-layered TMD flakes in Figure 2a also occur in monolayered (ML) flakes. Therefore, Figure 2c shows a

https://doi.org/10.1021/acsanm.1c03002
ACS Appl. Nano Mater. 2021, 4, 11305−11311

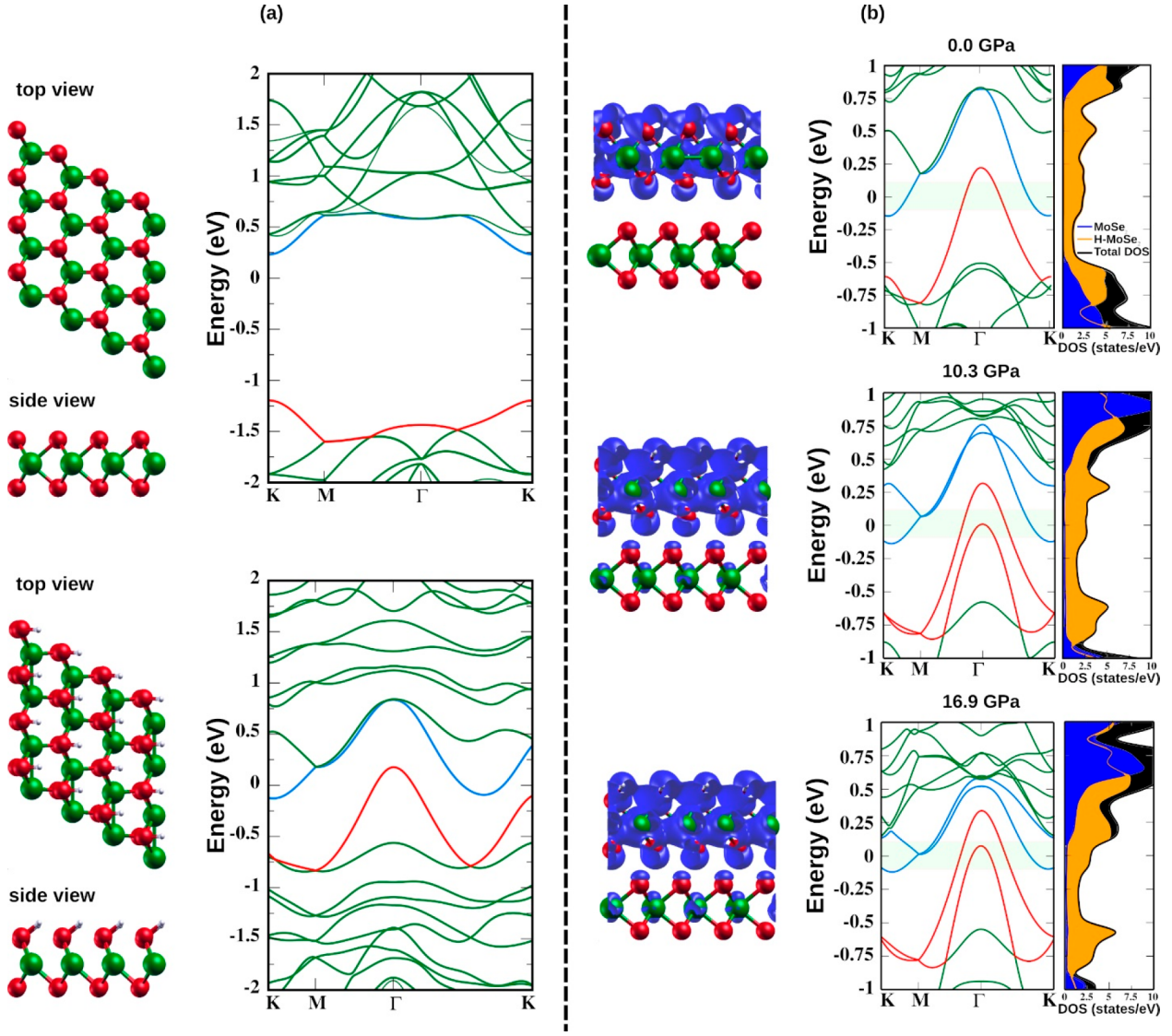

Figure 3. Changes in the electronic structure of the $MoSe_2$ under pressure. (a) Geometric models (two views) and corresponding band structures for monolayer $MoSe_2$. Pristine and H-functionalized cases are shown in the top and bottom panels, respectively. Red and blue lines in the band structures indicate valence band top and conduction band bottom, respectively. (b) Atomistic models for $MoSe_2$ bilayer in equilibrium interlayer distance (upper panel) and subjected to pressure (10.3 and 16.9 GPa for middle and bottom panels, respectively) and corresponding band structures and projected density of states (PDOS). Charge density plots corresponding to states indicated by gray stripes in the band plots (widths of 0.2 eV) are superimposed to the geometries. Red and blue lines in the band structures indicate Fermi-level crossing bands from both valence and conduction bands, respectively. In the PDOS, orange and blue curves correspond to projection onto the top H-functionalized and bottom layers, respectively, while the black curve is the total density of states. The Fermi level is set to zero in all plots.

similar experiment of Figure 2a directly comparing the charging efficiency of ML and FL $MoSe_2$ at the same environmental conditions. It is interesting to observe that qualitatively both ML (dark blue triangles) and FL (light blue squares) flakes present the same electromechanical modulations. There are two small quantitative differences though: the force onset for the second transition is smaller on the ML than in the FL flake, and the modulation amplitude (magnitude of charge efficiency variation) is larger for the ML than for the FL flakes. In other words, differently from electromechanical modifications in graphene and h-BN which require at least two layers to occur,[20,21] the electromechanical modifications in TMDs also occur in single-layer flakes.

Finally, the influence of two other environment-related parameters—atmosphere-related water contamination and temperature—on the observed pressure-induced transitions was investigated, and the results are shown in Figure 2d. Besides the initial environmental conditions of Figures 2a–c, a combination of dry atmosphere and different sample temperatures was also tested with the aid of a homemade environmental chamber and an *in situ* heating accessory (see the inset in Figure 2d). In this experiment, a FL MoS_2 flake was used to repeat the charging experiment of Figure 2a under three different temperatures (all at 0% RH N_2 atmosphere). Initially, at room temperature (T = 23 °C; green circles in Figure 2d) the two-step electromechanical modulation is reproduced as expected (it is essentially the same experiment of Figure 2a with more experimental points). However, when the sample temperature is raised to 120 °C (green triangles) and later to 180 °C (green diamonds), the initial transition (or first step) disappears, and a pronounced charging plateau is visible for F < 400 nN. Only the second transition at higher

https://doi.org/10.1021/acsanm.1c03002
ACS Appl. Nano Mater. 2021, 4, 11305−11311

force values is observed. Interestingly, we did not observe a well-defined plateau after the second transition within the force range available in the experiment. Nevertheless, the really intriguing question raised by the results in Figure 2d is the disappearance of the low-pressure transition at temperatures above 100 °C. At these temperatures and under a dry N_2 atmosphere, it is expected that most water molecules—from the ubiquitous contamination layer—should be desorbed from the TMD surface. In other words, the results in Figure 2d are a strong indication of the key role of water molecules for the occurrence of the first (low pressure) transition.

In summary, two of the most striking features in Figure 2 are the existence of two plateaus in charge injection efficiency as a function of applied force for all TMDs (ML and FL) and the disappearance of the low-pressure modification at high temperatures in a water-free environment. To account for such phenomenology, we propose a model based on a two-step process: in a first step, adsorbents on the sample surface play a key role since they provide chemical groups which may covalently bind to the chalcogen atoms on the upper surface of the TMDs in pressure-mediated processes. The reaction drives the topmost layer to a conductive state—a conductive band localized at this layer represents an electronic channel responsible for the increase in charge injection efficiency. This effect must vanish if the temperature is high enough to prevent the formation of an adsorbent layer on the sample. Second, upon increasingly pressure values, two effects may contribute to further enhance the density of states at the Fermi level: (1) intralayer deformations, which take place within the top hydrogenated layer (an effect common to both monolayer and few-layer systems) and modulate the electronic states at the Fermi level; (2) the increasing interlayer interaction, which occurs independently of the presence of adsorbents and makes multilayer TMDs undergo a semiconductor−metal transition. Taken together, the second mechanism contributes to additional bands at the Fermi level, increasing the charge injection efficiency.

The first mechanism is similar to the hydrogenation process reported by Han et al.,[14] which performed a systematic characterization of MoS_2 samples exposed to a hydrogen atmosphere at 300 °C and reported the formation of S−H bonds on the upper surface. The second mechanism has been extensively investigated in pristine multilayer TMDs.[10,23−26] In particular, the role of interlayer distance in bandgap modulation has been ascribed to changes in the energy of states at the top of the valence band. These states are linear combinations of sulfur p_z and molybdenum d_{z^2} orbitals,[25] and the effect eventually induces a semiconductor−metal transition.[26] Using $MoSe_2$ as an example, first-principles calculations[27,28] (employing a 2 × 2 unit cell) fully corroborate our two-step model based on the combined effect of these mechanisms (see the Supporting Information for DFT calculation details). We begin by addressing the first mechanism, showing that it leads to gap closure, and then we proceed to the combined effect and its consequence to the local density of states to interpret the experiment. To simulate the application of pressure, we perform constraint relaxations: the system is allowed to relax within a predefined vertical distance (a "hard-wall constraint"). This is achieved by constraining the displacements of the topmost and bottom-most sulfur atoms along the vertical direction. The corresponding pressure can be directly evaluated by the sum of the remanent vertical force components in one of the sulfur layers.

Figure 3a, on the left, shows two views of the atomistic models of $MoSe_2$ monolayer, both pristine (top) and with an upper surface completely functionalized with H atoms (bottom). We assume that this functionalization originates in reactions which occur under pressure involving water molecules found in the TMD surface in ambient conditions.[13−22] However, we emphasize that the surface reaction may have other outcomes (functionalization with −OH, for instance), including partial, rather than complete, coverages, which are also consistent with our model (see the Supporting Information for details and examples). In our discussion, we will focus on the hydrogenation since it provides a systematic scheme to investigate pressure effects. On the right, we show their corresponding band structures. Clearly, the functionalization introduces dispersive bands at the Fermi level (set to zero) and can be responsible for a sharp increase of efficiency in a charge injection experiment. Next, Figure 3b presents the results for the combined effect which gives rise to the second transition. Its left panels show three geometric models for the $MoSe_2$ bilayer with its upper S layer H-functionalized superimposed to isosurface plots corresponding to the electronic densities close to the Fermi level: the top model refers to the equilibrium configuration, and the middle and bottom ones refer to interlayer distances reduced to 2.66 and 2.50 Å, respectively, which correspond to applied pressures of 10.3 and 16.9 GPa. The corresponding band structures and density of states (DOS) are also shown on the right of Figure 3b. Two effects contribute to enhance the density of states at the Fermi level: the first one occurs due to deformations within the hydrogenated layer, and its signature is the modulation of a conduction band at the M point, which begins at 0.2 eV at zero pressure and touches the Fermi level for larger pressures, as clearly shown for P = 16.9 GPa (this effect is also observed in the monolayer case (see the Supporting Information), and we ascribe to it the second plateau in its charge injection curve).

The second effect involves also the bottom layer, and its signature may be found in a conduction band which is located approximately at 0.75 eV at the K point in the zero-pressure case. Upon pressure application, its energy greatly shifts toward lower energies, and it makes the second layer contribute to the density of states at the Fermi level, as shown by the blue curve in the DOS projection for P = 16.9 GPa in Figure 3b. The isosurface plots on the left corroborates our reasoning: the metallization process, in the zero-pressure case, is restricted to the upper layer, while the aforementioned additional bands, which show up close to the Fermi level as a response to the applied pressure, first enhance the contribution of the upper layer and, then, involve also the bottom layer. At this point, a pressure-induced metallization of the whole structure occurs. The overall effect furnishes more electronic channels which contribute to an increase in the charge injection efficiency. A similar reasoning should apply to all other TMDs investigated in this work, and in the Supporting Information, we present the MoS_2, WS_2, and WSe_2 cases.

In summary, the present work brings experimental and theoretical investigations on environment-related electro-mechanical modulations in four different TMD nanosheets (MoS_2, WS_2, $MoSe_2$, and WSe_2—monolayers and few layers). We show that three environmental parameters (pressure, atmosphere-related water, and temperature) can be used to dynamically tune the electrical response of these TMD

https://doi.org/10.1021/acsanm.1c03002
ACS Appl. Nano Mater. 2021, 4, 11305−11311

nanosheets into different states. Notwithstanding the physical insights unveiled by our results, it is their possible applicability that makes them stand out. Given the current widespread use of TMDs at the core of a wide variety of nanoscale sensors, it is natural to foresee a significant impact of this work on the design and operation of environment-related sensor devices, especially when a combination of pressure, temperature, and atmosphere is at play. For example, TMD-based stress sensors will have different electrical responses in humidity-rich environments or at high temperatures. Therefore, we believe the present work trails a few steps toward more comprehensive applications of the important class of transition metal dichalcogenide materials.

■ ASSOCIATED CONTENT

Supporting Information

The Supporting Information is available free of charge at https://pubs.acs.org/doi/10.1021/acsanm.1c03002.

Experimental details, effects of ambient relative humidity on the charging and discharging processes of TMDs, concomitant topographic and electrical images of a flake, influence of the number of layers on the charging efficiency of a flake, comparison between EFM and SKPM images, charge experiments sweeping the force up and down, topographic images of a TMD flake before charging, charged and after discharging, surface morphology of monolayered TMDs, possible effects of lateral strain due to thermal expansion on charging efficiency, theoretical calculation details, possible TMD functionalization reactions, stability aspects of functionalized TMDs, the monolayer case: pressure effect and the case of other TMDs: MoS_2, WS_2, and WSe_2 (PDF)

■ AUTHOR INFORMATION

Corresponding Author

Bernardo R. A. Neves − *Departamento de Física, Universidade Federal de Minas Gerais, 31270-901 Belo Horizonte, MG, Brazil;* orcid.org/0000-0003-0464-4754; Email: bernardo@fisica.ufmg.br

Authors

Mauricio V. Bessa − *Departamento de Física, Universidade Federal de Ouro Preto, 35400-000 Ouro Preto, MG, Brazil; Centro de Microscopia, Universidade Federal de Minas Gerais, 31270-901 Belo Horizonte, MG, Brazil*

Wellington D. Freitas − *Departamento de Física, Universidade Federal de Ouro Preto, 35400-000 Ouro Preto, MG, Brazil; Centro Federal de Educação Tecnológica de Minas Gerais, CEFET-MG, 30421-169 Belo Horizonte, MG, Brazil*

Natália P. Neme − *Departamento de Física, Universidade Federal de Ouro Preto, 35400-000 Ouro Preto, MG, Brazil; Zernike Institute for Advanced Materials and Stratingh Institute for Chemistry, University of Groningen, 9747 AG Groningen, The Netherlands*

Luiz G. P. Martins − *Physics Department, Massachusetts Institute of Technology, Cambridge, Massachusetts 02139, United States;* orcid.org/0000-0001-9777-7999

Ana P. M. Barboza − *Departamento de Física, Universidade Federal de Ouro Preto, 35400-000 Ouro Preto, MG, Brazil*

Matheus J. S. Matos − *Departamento de Física, Universidade Federal de Ouro Preto, 35400-000 Ouro Preto, MG, Brazil*

Mario S. C. Mazzoni − *Departamento de Física, Universidade Federal de Minas Gerais, 31270-901 Belo Horizonte, MG, Brazil*

Complete contact information is available at: https://pubs.acs.org/10.1021/acsanm.1c03002

Author Contributions

A.P.M.B., M.J.S.M., M.S.C.M., and B.R.A.N. proposed the project. M.V.B. and A.P.M.B. performed the experiments. W.D.F. and N.P.N. performed *ab initio* calculations under the supervision of M.J.S.M. and M.S.C.M. L.G.P.M. provided some TMD samples. M.J.S.M., M.S.C.M., and B.R.A.N. wrote the manuscript with input from all authors. All authors have given approval to the final version of the manuscript.

Author Contributions

M.V.B., W.D.F., and N.P.N. contributed equally to this work.

Notes

The authors declare no competing financial interest.

■ ACKNOWLEDGMENTS

The authors acknowledge financial support from CNPq, FAPEMIG, and INCT-Nano-Carbono. M.J.S.M. and A.P.M.B. acknowledge the support from Universidade Federal de Ouro Preto (UFOP). N.P.N., W.D.F., and M.V.B. acknowledge financial support from CAPES - Finance Code 001. L.G.P.M. acknowledges the support from AFOSR FATE MURI, Grant FA9550-15-1-0514, and the support from CNPQ under the program Ciência sem Fronteiras (206251/2014e9). We also acknowledge computational support from LCC-CENAPAD-UFMG and CESUP-UFRGS.

■ REFERENCES

(1) Novoselov, K. S.; Jiang, D.; Schedin, F.; Booth, T. J.; Khotkevich, V. V.; Morozov, S. V.; Geim, A. K. Two-dimensional atomic crystals. *Proc. Natl. Acad. Sci. U. S. A.* **2005**, *102*, 10451−10453.

(2) Wang, Q. H.; Kalantar-Zadeh, K.; Kis, A.; Coleman, J. N.; Strano, M. S. Electronics and optoelectronics of two-dimensional transition metal dichalcogenides. *Nat. Nanotechnol.* **2012**, *7*, 699−712.

(3) Choi, W.; Choudhary, N.; Han, G. H.; Park, J.; Akinwande, D.; Lee, Y. H. Recent development of two-dimensional transition metal dichalcogenides and their applications. *Mater. Today* **2017**, *20*, 116−130.

(4) Bhattacharyya, S.; Singh, A. K. Semiconductor-metal transition in semiconducting bilayer sheets of transition-metal dichalcogenides. *Phys. Rev. B: Condens. Matter Mater. Phys.* **2012**, *86*, 1−7.

(5) Kumar, A.; Ahluwalia, P. K. Electronic structure of transition metal dichalcogenides monolayers 1H-MX2 (M = Mo, W; X = S, Se, Te) from ab-initio theory: new direct band gap semiconductors. *Eur. Phys. J. B* **2012**, *85* (186), 1−7.

(6) Su, X.; Ju, W.; Zhang, R.; Guo, C.; Yong, Y.; Cui, H.; Li, X. Band gap modulation of transition-metal dichalcogenide MX2 nanosheets by in-plane strain. *Phys. E* **2016**, *84*, 216−222.

(7) Garcıa, A. M.; del Corro, E.; Kalbac, M.; Frank, O. Tuning the electronic properties of monolayer and bilayer transition metal dichalcogenide compounds under direct out-of-plane compression. *Phys. Chem. Chem. Phys.* **2017**, *19*, 13333−13340.

(8) Ram, B.; Singh, A. K. Strain-induced indirect-to-direct band-gap transition in bulk SnS2. *Phys. Rev. B: Condens. Matter Mater. Phys.* **2017**, *95*, 1−8.

(9) Fu, D.; Zhou, J.; Tongay, S.; Liu, K.; Fan, W.; Liu, T. J. K.; Wu, J. Mechanically modulated tunneling resistance in monolayer MoS2. *Appl. Phys. Lett.* **2013**, *103*, 183105.

(10) Nayak, A. P.; Bhattacharyya, S.; Zhu, J.; Liu, J.; Wu, X.; Pandey, T.; Jin, C.; Singh, A. K.; Akinwande, D.; Lin, J. F. Pressure-induced

semiconducting to metallic transition in multilayered molybdenum disulphide. *Nat. Commun.* **2014**, *5* (3731), 1−9.
(11) Chi, Z.-H.; Zhao, X. M.; Zhang, H.; Goncharov, A. F.; Lobanov, S. S.; Kagayama, T.; Sakata, M.; Chen, X. J. Pressure-Induced Metallization of Molybdenum Disulfide. *Phys. Rev. Lett.* **2014**, *113* (3), 1−5.
(12) Naumov, P. G.; ElGhazali, M. A.; Mirhosseini, H.; Süß, V.; Morosan, E.; Felser, C.; Medvedev, S. A. Pressure-induced metallization in layered ReSe2. *J. Phys.: Condens. Matter* **2018**, *30*, 035401.
(13) Shi, H.; Pan, H.; Zhang, Y. W.; Yakobson, B. I. Strong ferromagnetism in hydrogenated monolayer MoS2 tuned by strain. *Phys. Rev. B: Condens. Matter Mater. Phys.* **2013**, *88* (20), 1−6.
(14) Han, S. W.; Yun, W. S.; Lee, J. D.; Hwang, Y. H.; Baik, J.; Shin, H. J.; Lee, W. G.; Park, Y. S.; Kim, K. S. Hydrogenation-induced atomic stripes on the 2H-MoS2 surface. *Phys. Rev. B: Condens. Matter Mater. Phys.* **2015**, *92* (24), 1−5.
(15) Wang, Y.; Ding, Y. The hydrogen-induced structural stability and promising electronic properties of molybdenum and tungsten dinitride nanosheets: a first-principles study. *J. Mater. Chem. C* **2016**, *4*, 7485−7493.
(16) Pierucci, D.; Henck, H.; Ben Aziza, Z.; Naylor, C. H.; Balan, A.; Rault, J. E.; Silly, M. G.; Dappe, Y. J.; Bertran, F.; Le Fevre, P.; Sirotti, F.; Johnson, A. T. C.; Ouerghi, A. Tunable Doping in Hydrogenated Single Layered Molybdenum Disulfide. *ACS Nano* **2017**, *11*, 1755−1761.
(17) Han, S. W.; Cha, G. B.; Park, Y.; Hong, S. C. Hydrogen physisorption based on the dissociative hydrogen chemisorption at the Sulphur vacancy of MoS2 surface. *Sci. Rep.* **2017**, DOI: 10.1038/s41598-017-07178-9.
(18) Ma, K. Y.; Yoon, S. I.; Jang, A-R.; Jeong, H. Y.; Kim, Y.-J.; Nayak, P. K.; Shin, H. S. Hydrogenation of monolayer molybdenum diselenide via hydrogen plasma treatment. *J. Mater. Chem. C* **2017**, *5* (43), 11294−11300.
(19) Barboza, A. P. M.; Gomes, A. P.; Archanjo, B. S.; Araujo, P. T.; Jorio, A.; Ferlauto, A. S.; Mazzoni, M. S.; Chacham, H.; Neves, B. R. A. Deformation Induced Semiconductor-Metal Transition in Single Wall Carbon Nanotubes Probed by Electric Force Microscopy. *Phys. Rev. Lett.* **2008**, *100* (25), 1−4.
(20) Barboza, A. P. M.; Guimaraes, M. H. D.; Massote, D. V. P.; Campos, L. C.; Barbosa Neto, N. M.; Cancado, L. G.; Lacerda, R. G.; Chacham, H.; Mazzoni, M. S. C.; Neves, B. R. A. Room-Temperature Compression-Induced Diamondization of Few-Layer Graphene. *Adv. Mater.* **2011**, *23*, 3014−3017.
(21) Barboza, A. P. M.; Matos, M. J. S.; Chacham, H.; Batista, R. J. C.; de Oliveira, A. B.; Mazzoni, M. S. C.; Neves, B. R. A. Compression-Induced Modification of Boron Nitride Layers: A Conductive Two-Dimensional BN Compound. *ACS Nano* **2018**, *12*, 5866−5872.
(22) Barboza, A. P.M.; Souza, A. C. R.; Matos, M. J. S.; Brant, J. C.; Barbosa, T. C.; Chacham, H.; Mazzoni, M. S.C.; Neves, B. R. A. Graphene/h-BN heterostructures under pressure: From van der Waals to covalent. *Carbon* **2019**, *155*, 108−113.
(23) Johari, P.; Shenoy, V. B. Tuning the Electronic Properties of Semiconducting Transition Metal Dichalcogenides by Applying Mechanical Strains. *ACS Nano* **2012**, *6*, 5449−5456.
(24) Scalise, E.; Houssa, M.; Pourtois, G.; Afanas'ev, V.; Stesmans, A. Strain-induced semiconductor to metal transition in the two-dimensional honeycomb structure of MoS2. *Nano Res.* **2012**, *5*, 43−48.
(25) Li, T.; Galli, G. Electronic Properties of MoS2 Nanoparticles. *J. Phys. Chem. C* **2007**, *111*, 16192−16196.
(26) Kumar, A.; Ahluwalia, P. K. Semiconductor to metal transition in bilayer transition metals dichalcogenides MX2 (M = Mo, W; X = S, Se, Te). *Modell. Simul. Mater. Sci. Eng.* **2013**, *21*, 065015.
(27) Kohn, W.; Sham, L. J. Self-consistent equations including exchange and correlation effects. *Phys. Rev.* **1965**, *140* (4A), A1133−A1138.
(28) Soler, J. M.; Artacho, E.; Gale, J. D.; García, A.; Junquera, J.; Ordejón, P.; Sánchez-Portal, D. The siesta method for ab initio order-n materials simulation. *J. Phys.: Condens. Matter* **2002**, *14* (11), 2745−2779.

https://doi.org/10.1021/acsanm.1c03002
ACS Appl. Nano Mater. 2021, 4, 11305−11311